

## High $\beta$ electron micro-stability in Spherical Tokamaks

N J Joiner<sup>1</sup>, D J Applegate<sup>1</sup>, S C Cowley<sup>2</sup>, W Dorland<sup>3</sup>, C M Roach<sup>4</sup>

<sup>1</sup>Imperial College, London, UK, <sup>2</sup>UCLA, Los Angeles, USA, <sup>3</sup>University of Maryland, College Park, USA, <sup>4</sup>EURATOM/UKAEA Fusion Association, Abingdon, UK

### Introduction

High  $\beta$  values achieved in spherical tokamaks, make experimental devices such as MAST [1] an attractive alternative route to fusion energy. Whether this can be realised depends on the underlying anomalous transport, and so understanding the behaviour of the micro-instabilities responsible for transport in these plasmas is very important. Electron scale micro-instabilities are investigated using the gyro-kinetic code, GS2 [2]. Variations of  $\beta' = -\beta/L_p$  and global magnetic shear  $\hat{s}$  are treated by a perturbative local equilibrium expansion [3] around MAST equilibrium flux surfaces [4]. In this way, linear stability is studied in regimes of steep pressure gradient and high local  $\beta$ .

### Equilibrium Effects

A scan of the normalised pressure gradient  $\alpha = -q^2 R\beta'$  is carried out for various values of the magnetic shear  $\hat{s}$ . The  $\rho = \psi/\psi_{LCFS} = 0.4$  surface is used for analysis, and the parallel magnetic perturbation is taken to be zero. Ions are treated as adiabatic, and the plasma is taken to be collisionless.

Taking  $k_y \rho_e = 0.6$  and decreasing the pressure gradient scale length (increasing the pressure gradient  $\alpha$ ) consistently between the equilibrium and gyro-kinetic equation, for the cases of finite  $\eta_e = const.$  and  $\nabla n = 0$ , reveals the destabilisation and subsequent stabilisation of multiple electron scale micro-instabilities (Figure 1), with  $\beta_e = const. = 0.05$  and  $\hat{s} = 2.0$ . Discontinuities in the plots of the real frequency indicate a change to a different mode or branch. Examination of the real frequency spectrum, for the  $\nabla n = 0$  scenario, in Figure 2 shows that an increase in  $\alpha$  brings about a more dominant mode at progressively longer perpendicular wavelengths.

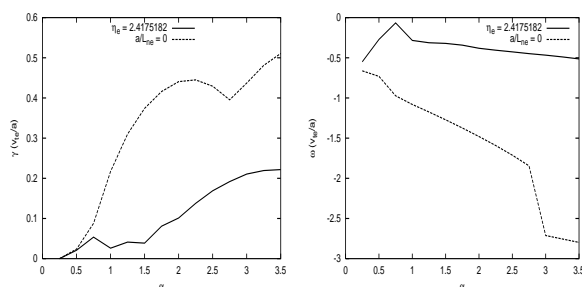


Figure 1: Growth rate  $\gamma$  vs.  $\alpha$ , and real frequency  $\omega$  vs  $\alpha$  for  $\eta_e = 2.42$  and  $\nabla n = 0$  with  $\hat{s} = 2.0$

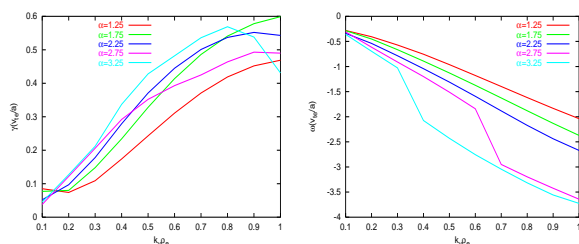


Figure 2:  $k_y$  spectrum for a series of  $\alpha$  ( $\hat{s} = 2.0, \nabla n = 0$ ) showing the transition between two branches as  $\alpha$  is increased

The eigenfunctions of the two branches reveal a possible explanation for the branch change in Figure 1. Figure 3 shows the eigenfunctions for the electrostatic potential at  $\alpha = 2.0$  and 3.0. The increased pressure gradient can

destabilise higher parallel harmonics, giving the eigenfunction more parallel structure.

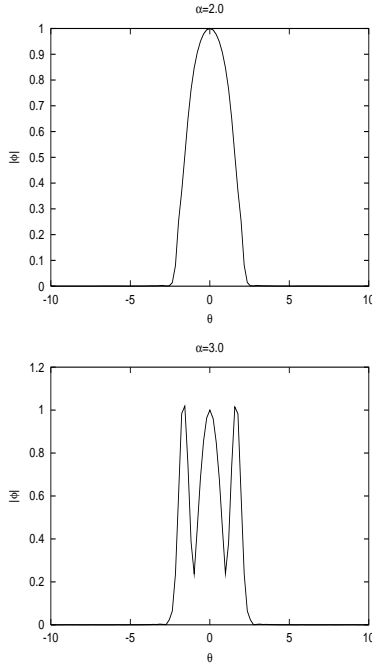


Figure 3:  $|\phi|$  vs.  $\theta$  for  $\alpha = 2.0$  and  $3.0$  ( $\hat{s} = 2.0, \nabla n = 0$ )

are  $\beta = 0.3$ ,  $\hat{s} = 1.3$ ,  $\eta_e = 3$ ,  $k_\theta \rho_e = 0.3$ . Figure 2 suggests that their use of lower  $k_y$  than the current work, may reduce the sensitivity of the pressure gradient on the growth rate.

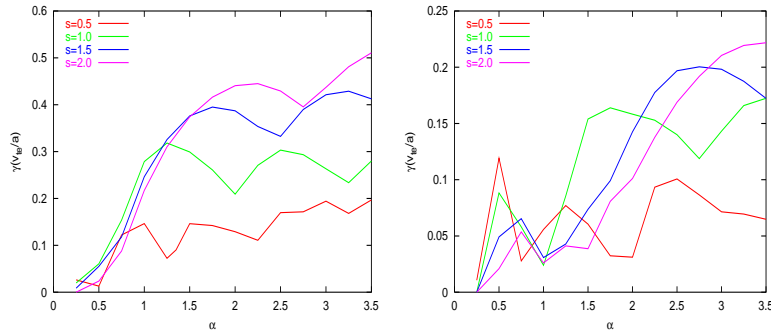


Figure 4: The effect of the pressure gradient on  $k_y \rho_e = 0.6$  for  $\hat{s} = 0.5, 1.0, 1.5, 2.0$ ,  $\nabla n = 0$  (left) and  $\eta_e = 2.4$  (right)

### $\beta$ effects

In this section the effect of  $\beta$  on the linear modes is investigated. We begin by varying  $\beta$  inconsistently with the equilibrium, in order to establish the electromagnetic effects on the ETG mode. Keeping to the  $\rho = 0.4$  surface of the MAST equilibrium, using the fully electromagnetic terms of GS2, figure 5 shows that  $\beta$  has a stabilising influence on the ETG mode.

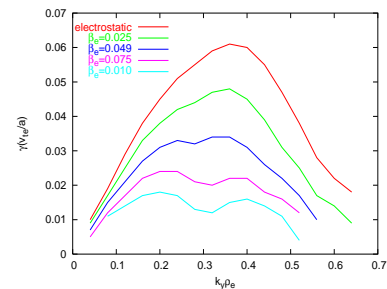


Figure 5: Growth rate vs.  $k_y$  for varying values of  $\beta_e$ , on the  $\rho = 0.4$  flux-surface

Figure 4 shows that this effect occurs at different values of the global magnetic shear, for both the finite  $\eta_e$  case and the  $\nabla n = 0$  case. The dispersion relation has been examined for a wide range of  $\hat{s}$  and  $\alpha$ , and shows a characteristic ETG curve. This work shows that there can be several different ETG branches characterised by the stability of their parallel components. The two competing effects of increasing  $\alpha$  are: first to move the longer parallel wave lengths into a regime of second stability, and secondly to provide the energy to destabilise shorter parallel wavelengths. Similar research on a NSTX plasma [5] shows one well defined peak in the growth rate of the ETG mode in a  $\beta'$  scan for the fully electromagnetic case, and two peaks when  $\delta B_{\parallel} = 0$  (The form of which bears a strong resemblance to the  $\hat{s} = 1.5$  curve in the left diagram of Figure 4). The parameters used by Bourdelle et. al [5]

Contrary to the conventional wisdom, that  $\delta B_{\parallel}$  can be neglected at low  $\beta$ , the  $\beta$  effect comes from  $\delta B_{\parallel}$  even at  $\beta_e = 0.025$  (Figure 6)

The lack of  $\beta$  effect from the  $A_{\parallel}$  terms can be explained to some extent by considering the local dispersion relation. This can be derived [6] with  $\delta B_{\parallel} = 0$ , using the gyro-kinetic equation, the quasi-neutrality condition and the parallel component of Ampère's law, giving,

$$1 + \tau - P_0 + \frac{P_1^2}{2k_{\perp}^2/\beta_e + P_2} = 0 \quad (1)$$

where,

$$P_m = \frac{1}{\sqrt{2\pi}} \int (v_{\parallel})^m \frac{\omega - \omega_* [1 + \eta_e(v^2/2 - 3/2)]}{\omega - \omega_D - k_{\parallel} v_{\parallel}} J_0^2(k_{\perp} v_{\perp}) e^{-v^2/2} v_{\perp} dv_{\perp} dv_{\parallel} \quad (2)$$

$\tau = T_e/T_i$ ,  $\beta_e = 8\pi n_0 T_e/B^2$ ,  $\omega_* = k_y$  and  $\omega_D = \epsilon_n \omega_* (v_{\parallel}^2 + v_{\perp}^2)$ . The wave numbers  $k_{\perp}$  and  $k_{\parallel}$  are normalised to the electron gyro-radius  $\rho_e = v_{te}/\Omega_{ce}$  and density gradient scale length  $L_n$  respectively. Frequencies are normalised to  $v_{te}/L_n$ .

As noted by Kim and Horton [6], when  $k_{\parallel} = 0$ , the integrand of  $P_1$  is odd in  $v_{\parallel}$ , and so  $P_1 = 0$  and the electromagnetic contribution disappears.

We have examined the  $k_{\parallel}$  power spectra for these eigenfunctions, and see that they are dominated by small parallel wavenumbers, which are unaffected by the electromagnetic term of equation 1. This illustrates how a local analysis at high  $k_{\parallel}$  [6] may overestimate the impact of  $\beta$ .

We have used the analytic methods of Kim and Horton [6] to obtain a dispersion relation for the ETG mode with finite  $\delta B_{\parallel}$  and  $A_{\parallel} = 0$ , and find that the electromagnetic term in this case is significant at low  $k_{\parallel}$ .

The above findings, have also been seen on the  $\rho = 0.6$  and  $0.8$  surfaces, and in simulations on high aspect ratio, low  $\beta$ , analytic equilibria.

### Micro-tearing

Electromagnetic modes with tearing parity in the eigenfunctions have been observed to occur for  $\hat{s} \gtrsim 1$  and  $a/L_p \gtrsim 3$  at  $k_y \rho_e \sim 0.01-0.15$ . The importance of these collisionless electron-tearing modes is illustrated in a conceptual Spherical Tokamak Power Plant (STPP) [7], where the ETG mode is found to be absolutely stabilised, leaving

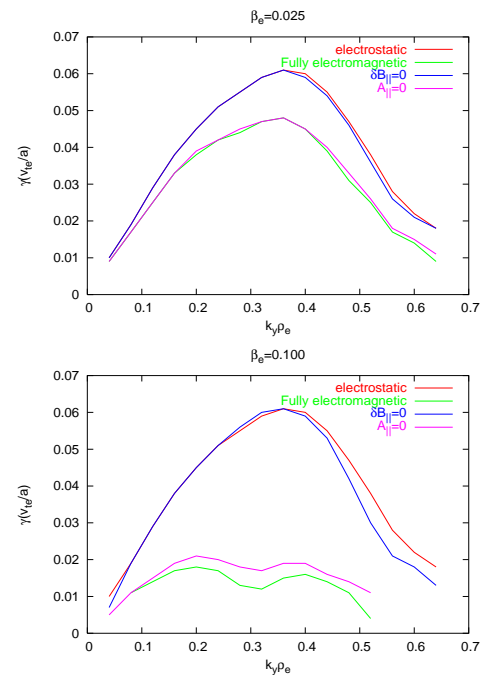


Figure 6: Comparison of the effects of  $A_{\parallel}$  and  $\delta B_{\parallel}$  for  $\beta_e = 0.025$  and  $\beta_e = 0.100$

micro-tearing modes as the dominant instabilities. A Poincaré sectioning diagnostic (Figure 7) as been developed to show the evolution of the confining magnetic field to stochasticity from magnetic island growth.

### Nonlinear Simulation

A nonlinear study has begun, to establish the effect of high  $\beta$  on turbulent ETG transport (Figure 8), and the significance of the micro-tearing mode, using EPSRC's HPCx and USDOE's Cheetah high performance computers.

The early results show experimentally significant transport, though convergence studies of the result in Figure 8 with respect to the  $x$  and  $y$  wavenumbers and flux-tube width have yet to be completed.

Preliminary studies of the tearing mode show that magnetic transport is the dominant mechanism.

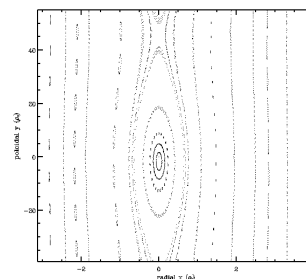


Figure 7: Islands produced by the micro-tearing modes visualised by Poincaré section

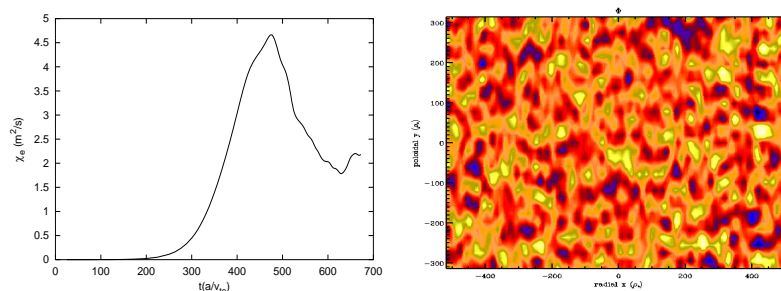


Figure 8: Nonlinear MAST simulation. Thermal diffusivity vs time (left) and contours of electrostatic potential ( $\theta = 0$ ) (right)

### References

- [1] A.Sykes et al. Phys.Plasmas **8**, 2101 (2001).
- [2] M.Kotschenreuther, G.Rewoldt and W.M.Tang, Comp.Phys.Comm. **88**, 128 (1995).
- [3] J.M.Greene and M.S.Chance, Nucl.Fusion **4**, 453 (1981).
- [4] D.Applegate et al. 31st EPS conf. of Cont. Fusion and Plasma Phys, London (2004)
- [5] C.Bourdelle et al. Phys.Plasmas **10**, 2881, (2003).
- [6] J.Y. Kim and W.Horton Phys.Fluids **B3**, 3194, (1991).
- [7] H.R.Wilson et al. submitted to Nucl.Fusion

*This work is funded by the UK Engineering and Physical Sciences Research Council  
The authors would like to thank Jack Connor for helpful discussion*